

Determination of Early Flow Stress for Ductile Specimens at High Strain Rates by Using a SHPB

B. Song · W. Chen · B.R. Antoun · D.J. Frew

Received: 6 August 2006 / Accepted: 14 March 2007 / Published online: 27 April 2007
© Society for Experimental Mechanics 2007

Abstract In a dynamic experiment to obtain the high-rate stress–strain response of a ductile specimen, it takes a finite amount of time for the strain rate in the specimen to increase from zero to a desired level. The strain in the specimen accumulates during this strain-rate ramping time. If the desired strain rate is high, the specimen may yield before the desired rate is attained. In this case, the strain rates at yielding and early plastic flow are lower than the desired value, leading to inaccurate determination of the yield strength. Through experimentation and analysis, we examined the validity and accuracy of the flow stresses for ductile materials in a split Hopkinson pressure (SHPB) bar experiment. The upper strain-rate limit for determining the dynamic yield strength of ductile materials with a SHPB is identified.

Keywords Split Hopkinson pressure bar (SHPB) · Ductile materials · Constant strain rates · Flow stress · Yield strength

Introduction

Development of accurate rate-dependent material models for the purpose of engineering design and optimization in a variety of applications where high-rate loading is encountered

requires reliable materials properties determined by experiments over a wide range of strain rates [1]. This practical need has attracted extensive modeling efforts [2–4]. For example, strain-rate effects on flow stress/yield strength have been examined for a number of ductile materials [5–10]. The flow stress beyond plastic yielding at low strain rates can be precisely determined at specified rates from conventional quasi-static experiments. In such quasi-static experiments, the testing conditions can typically be controlled without considering the specimen response due to high machine rigidity. By contrast, the testing conditions in dynamic experiments with Hopkinson bars, which are much less rigid, are much more difficult to control for achieving desired testing conditions. Pulse shaping technique extensively developed in recent decades makes dynamic testing conditions more controllable in split Hopkinson pressure bar (SHPB) experiments [11, 12]. The pulse shaping technique was originally developed as a pulse smoother [13]. During the most recent decade, the main function of the pulse shaping technique has been turned to produce a desired profile of incident pulse to ensure dynamic stress equilibrium and constant strain-rate deformation in specimen. Chen et al. [14] conducted dynamic compressive experiments on a mild steel with and without pulse shaping technique. Their results show that early stress–strain data before yielding from a non-pulse-shaped experiment is not valid due to non-equilibrated stress state in specimen. However, valid data at small strains are obtained by using the pulse shaping technique. The pulse shaping technique also facilitates constant strain-rate deformation in specimen. There is a nature that it takes time to accelerate a specimen at rest to a steady-state dynamic deformation. In a SHPB experiment, as the desired strain rates increase, the time for the loading process to reach a certain strain in a specimen during an experiment becomes shorter and shorter. From this phenomenon, there are two

B. Song (SEM member) · W. Chen (✉, SEM member)
Schools of AAE and MSE, Purdue University,
West Lafayette, IN 47907-2023, USA
e-mail: wchen@purdue.edu

B.R. Antoun
Sandia National Laboratories,
Livermore, CA 94551-0969, USA

D.J. Frew (SEM member)
Sandia National Laboratories,
Albuquerque, NM 87184-1174, USA

issues that would need attention in experimental design. First, it is noted that the strain in the specimen accumulates during this ramping-up time. It is possible that the accumulated strain in the ductile specimen before the strain rate reaches a desired constant value is enough to reach the yield strain. In this case, the yield strength is actually determined at the lower strain rate than the claimed constant value. Therefore, using the obtained yield strength and the claimed constant strain-rate data to study the strain-rate effects for materials, especially for rate-sensitive materials, is certainly not acceptable. As the desired rate further increases, this situation expands to early plastic-flow region of the ductile specimen's stress-strain behavior. Second, as the desired strain rate increases, the rise time in the loading pulse needs to be shorter and shorter. In a SHPB experiment, the rise time cannot be infinitely small. It is therefore necessary to examine in detail the conditions under which the dynamic yielding and flow behaviors are obtained. While this uncertainty in dynamic experimental results described here can occur in many high-rate experiments under tension, torsion, or compression conditions, in this paper, we take the case of a SHPB experiment to explore the limiting conditions under which a valid experiment can be performed.

The SHPBs are used to determine the dynamic compressive responses of engineering materials, including ductile materials, in the strain-rate range from 10^2 to 10^4 s^{-1} [15, 16]. To obtain a family of dynamic stress-strain curves as a function of strain rate with the SHPB, the strain rate in the specimen is desired to be a constant during each experiment, which is not automatically achieved in a conventional SHPB experiment [14, 17]. Variations in strain rates during a SHPB experiment have been demonstrated to significantly affect the resultant stress-strain data, especially for the rate-sensitive materials [18–20]. For example, Kobayashi et al. [19] investigated the effect of strain rate change on instability strain (the strain at the maximum load) during SHPB dynamic tensile tests for a 0.45% steel. The instability strain was found to be very sensitive to the strain rate history in specimen. As compared to constant rate of deformation, the acceleration in specimen deformation resulted in the larger instability strain whereas the decelerated specimen deformation led to the smaller value of instability strain. Nojima and Ogawa [20] also pointed out that the true material response is often veiled by varied strain rate during a SHPB test. In hence, it is essential to deform a specimen, particularly a strain-rate-sensitive specimen, at a constant strain rate over the entire loading duration such that the true strain-rate effects of the specimen enable to be revealed. As mentioned earlier, the pulse shaping techniques have made the SHPB more controllable. The SHPBs modified with proper pulse shaping designs have demonstrated the capabilities of characterizing dynamic stress-strain behavior of various

materials at constant strain rates [21, 22]. In particular, Frew et al. [12] developed composite pulse shapers for achieving constant strain rates during dynamic loading on high-strength ductile steels. Although pulse shaping techniques ensure the specimen to deform at nearly constant strain rates over most of loading duration, the constant-rate is typically not maintained during the early stages of the dynamic loading. At the beginning of a dynamic experiment, it always takes time for the strain rate in the specimen to increase from zero to the constant level. The strain in the specimen accumulated in this time may exceed the yield strain (<0.01 for most metals) before a constant strain rate is reached if the desired constant level is sufficiently high.

Similar phenomenon has also been observed in the SHPB experiments on elastic brittle specimens (S-2 glass/SC15 composite and PMMA), where specimens failed before the desired constant strain rates were reached [23]. There exists an upper limit for achievable constant strain rates in SHPB experiments on those materials. When characterizing metallic materials at high rates, which also have elastic behavior before yielding, it is also necessary to examine if there is an upper limit in strain rates beyond which constant strain rate cannot be achieved at yielding.

In this study, we examine the yield strength and early plastic flow stress for a 4340 steel and an HP9-4-20 steel alloy at high strain rates with a pulse-shaping SHPB. A strain-rate dependent material model is modified to describe the effects of strain-rate variation on the yield strength and early plastic flow stress the 4340 steel.

The Modified SHPB for Characterizing Ductile Materials

A conventional SHPB device typically consists of a gas gun, a striker, an incident bar, a transmission bar, a momentum absorption device, and a data acquisition system. The specimen is sandwiched between the incident bar and the transmission bar. The impact of the striker, which is launched by the compressed gas in the gas gun, on the end of the incident bar generates an elastic wave (incident wave) that propagates through the incident bar. When the incident wave travels to the specimen, the specimen is compressed. Due to the mechanical impedance mismatch between the bars and the specimen, part of the incident wave is reflected back into the incident bar as a reflected wave and the rest transmits into the transmission bar as a transmitted wave. A valid SHPB experiment requires the specimen to be in a state of uniform stress over the loading duration. Under dynamically equilibrated stresses, one dimensional wave analysis yields the strain

rate, strain, and stress histories in the specimen as the follows [5, 16],

$$\dot{\varepsilon}(t) = -2 \frac{C_0}{L_s} \varepsilon_r(t) \quad (1)$$

$$\varepsilon(t) = -2 \frac{C_0}{L_s} \int_0^t \varepsilon_r(t) dt \quad (2)$$

$$\sigma(t) = \frac{A_0}{A_s} E_0 \varepsilon_t(t) \quad (3)$$

where $\varepsilon_r(t)$ and $\varepsilon_t(t)$ are reflected and transmitted strain histories, respectively; A_0 is the cross-sectional area of the bars; E_0 and C_0 are Young's modulus and elastic bar wave speed in the bar material, respectively; A_s and L_s are initial cross-sectional area and length of the specimen, respectively. Therefore, the strain and stress histories in the specimen under investigation are calculated from the reflected and transmitted signals, respectively, such that the dynamic stress–strain curves are obtained. It is emphasized again that the dynamic stress equilibrium can be physically achieved through pulse shaping technique such that equations (1)–(3) are applicable to calculate the resultant stress and strain data. Using three-wave analysis instead of pulse shaping technique can artificially smoothen out the severe stress and strain gradients in the specimen, which provides superficially good looking results. However, the three-wave analysis does not provide a solution to the fundamental problem of non-uniform deformation of the specimen.

To properly delineate the strain-rate effects for a specific material, the strain rate in the specimen during each SHPB experiment needs to be approximately maintained at a constant over the loading duration. A family of such stress–strain curves obtained at various constant strain rates facilitate the quantitative investigation on strain-rate effects. A constant strain-rate history in a specimen during a SHPB experiment is indicated by a plateau in the reflected pulse under dynamically equilibrated stresses [equation (1)]. However, in a conventional SHPB experiment, the strain rate often decreases due to work hardening response of the metal specimen. A SHPB modified with double pulse shaping design has been demonstrated to be capable of obtaining the stress–strain curves for ductile materials at constant strain rates [12, 14]. The proper pulse shaping technique enables to obtain accurate measurements at small strains for metals [14] and dynamic elastic and early cell-collapse responses at small strains for a polystyrene foam [24].

Dynamic Experiments with the Modified SHPB

Dynamic compression experiments on a 4340 HRC45 steel, provided by Sandia National Laboratories, Albuquerque, NM, were conducted with a SHPB modified with double pulse shapers, the schematic of which is shown in Fig. 1. The striker, incident, and transmission maraging steel bars had a common diameter of 19.05 mm. The specimens are 9.53 mm in diameter and 6.35 mm in length. In the pulse-shaped SHPB experiment, the composite pulse shapers that consist of a partially annealed C11000 copper disk and a 4340 HRC30 steel cylinder were placed on the impact end of the incident bar. Upon the impact of the striker, the pulse shapers were extensively compressed, generating a different profile of the incident pulse from that obtained in a conventional Hopkinson bar experiment. If the dimensions of the pulse shapers are appropriately selected, the profile of the incident pulse is controlled to ensure that the specimen deforms at a nearly constant strain rate under dynamic stress equilibrium [12, 14]. Besides the pulse shapers on the impact end of the incident bar, two M2 tool steel platens with the same diameter as the bars were attached to the specimen ends of the incident and transmission bars, respectively, to protect the bar ends from indentation damage caused by the hard specimen.

As mentioned in the “Introduction” Section, during a dynamic compressive experiment, the strain rate in the specimen increases from zero to a desired level. Proper pulse shaping techniques ensure the eventual strain rate to remain at a constant level over the most of the experiment duration. The dynamic compression experiments presented here were conducted at three eventual strain rates: 5.8×10^2 , 1.7×10^3 , and $3.6 \times 10^3 \text{ s}^{-1}$. Figure 2 shows a typical set of incident, reflected, and transmitted oscilloscope records which were obtained from an experiment at the strain rate of $1.7 \times 10^3 \text{ s}^{-1}$. The incident pulse in Fig. 2 clearly has a different profile from those obtained from conventional SHPB experiments. This is the result of employing the pulse shapers at the impact end of the incident bar. In a SHPB experiment, the specimen's response significantly affects the testing conditions. For example, if a step incident is used to load a ductile work-hardening specimen, the rate of the deformation will inevitably decrease as the

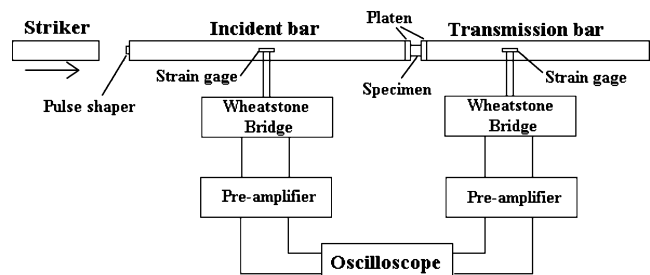


Fig. 1 A schematic of pulse-shaping SHPB setup

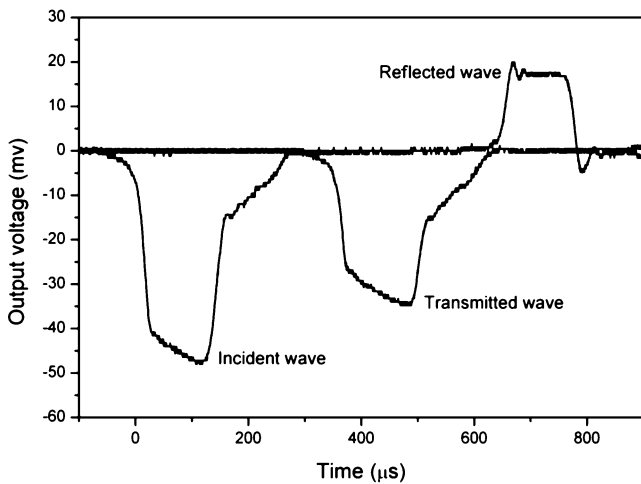


Fig. 2 A typical set of incident, reflected, and transmitted pulses for the 4340 steel specimen at the strain rate of $1.7 \times 10^3 \text{ s}^{-1}$

specimen work hardens. This is because the loading is maintained at a constant, which is unable to deform the hardened specimen as fast. To maintain a constant strain rate, the amplitude of the loading pulse must increase (pulse shaping) as the deformation in the specimen increases. Therefore, pulse shaping is necessary to ensure constant-strain-rate testing conditions. Furthermore, due to the nature of wave propagation in a dynamic experiment, the front of a loading pulse cannot be very steep in order to allow the specimen to deform under a dynamically equilibrated stress, which is a required condition in any experiment for material characterization. Thus, equilibrium requirement also calls for proper pulse shaping in a valid Hopkinson bar experiment. The modified incident pulse through pulse shaping technique shown in Fig. 2 facilitates dynamic stress equilibrium in a specimen over the entire loading duration, as shown in Fig. 3. Figure 3 shows the axial force histories at the front (in contact with the incident bar) and the back (in contact with the transmission bar) ends of the metal specimen loaded by the incident pulse shown in Fig. 2. The nearly overlapping histories clearly indicate that the axial stresses in the specimen are approximately equilibrated over the entire dynamic loading duration. Under dynamic stress equilibrium, the strain rate history is proportional to the reflected pulse [equation (1)]. The plateau in the reflected pulse in Fig. 2 thus indicates the nearly constant strain-rate deformation in the specimen. It should be noted that, when the strain in the specimen is excessively large, a true strain rate to describe the specimen behavior may become necessary [25]. In that case, a plateau in the reflected pulse may not indicate a constant true strain rate in the specimen. However, in this research, our focus is on the accuracy of experimental data associated with the early plastic deformation. We only maintained engineering strain rate to be constant in the experiments reported in this paper.

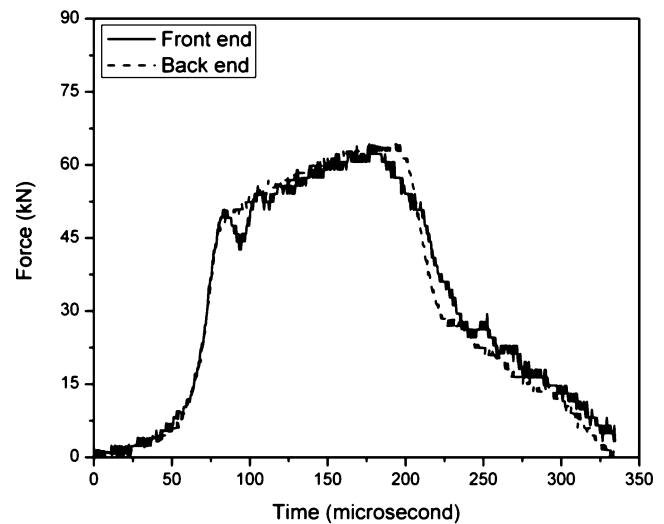


Fig. 3 Dynamic stress equilibrium in specimen

To examine the strain history together with the strain rate history for the purpose of determining the strain at which the strain rate reaches constant, the strain-rate and strain histories at the strain rate of $1.7 \times 10^3 \text{ s}^{-1}$ are shown in Fig. 4. An examination of Fig. 4 indicates that it took approximately $90 \mu\text{s}$ for the strain rate to increase from zero to the constant value of $1.7 \times 10^3 \text{ s}^{-1}$. Note that the slight oscillation, which inevitably occurs when the specimen material is very hard, in the strain rate is neglected. In this first $90 \mu\text{s}$, the specimen has accumulated a true strain of 0.026, as marked by the horizontal dotted line in Fig. 4, which far exceeds the yield strain of the specimen material. This fact indicates that the stress–strain data within the strain of 0.026 were obtained at the increasing strain rates rather than the claimed constant strain rate ($1.7 \times 10^3 \text{ s}^{-1}$). Figure 5 shows the strain-rate and strain histories in the specimen at the strain rate of $3.6 \times 10^3 \text{ s}^{-1}$ where a similar but more severe phenomenon is observed. The strain rate

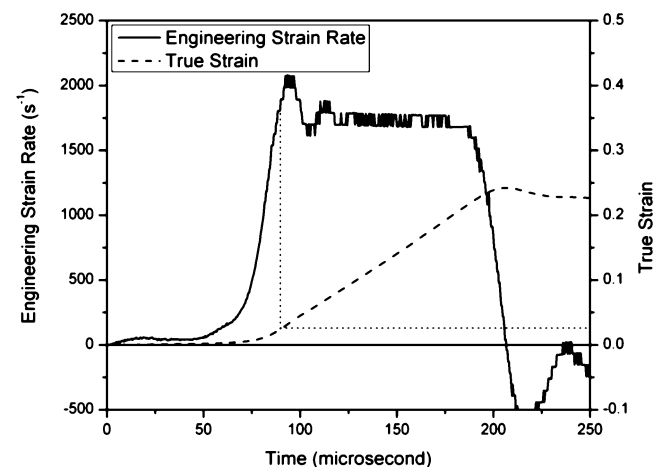


Fig. 4 Engineering strain-rate and true strain histories in specimen at the strain rate of $1,700 \text{ s}^{-1}$

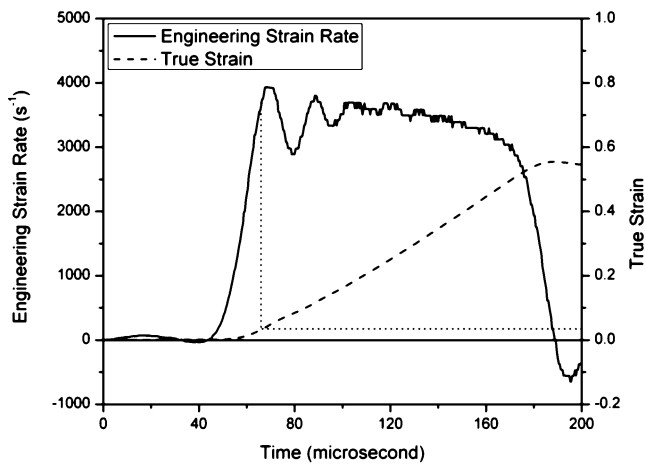


Fig. 5 Engineering strain-rate and true strain histories in specimen at the strain rate of $3,600 \text{ s}^{-1}$

was increasing from zero to $3.6 \times 10^3 \text{ s}^{-1}$ during the first $66 \mu\text{s}$ that corresponds to a strain of 0.035. This phenomenon cannot be avoided while conducting experiments at high strain rates. As the eventual constant strain rate decreases, the situation becomes less severe. For example, at the strain rate of $5.8 \times 10^2 \text{ s}^{-1}$, the accumulated strain in the specimen before the strain rate reaches the constant value ($5.8 \times 10^2 \text{ s}^{-1}$) is less than 0.015. In this case, it may be acceptable to consider that all of the plastic deformation was obtained at the constant strain rate ($5.8 \times 10^2 \text{ s}^{-1}$). It has been demonstrated that the strain rate of elastic deformation was approximately two orders lower than the plastic strain rate in a SHPB experiment [14].

In order to examine the strain-rate effects and to develop a strain-rate-dependent material model over a wider range of strain rates, we also conducted the quasi-static experiments at the strain rates of 3.4×10^{-4} , 3.4×10^{-3} , and $3.4 \times 10^{-2} \text{ s}^{-1}$ with a standard MTS machine. Figure 6 shows the resultant stress–strain curves obtained from both dynamic

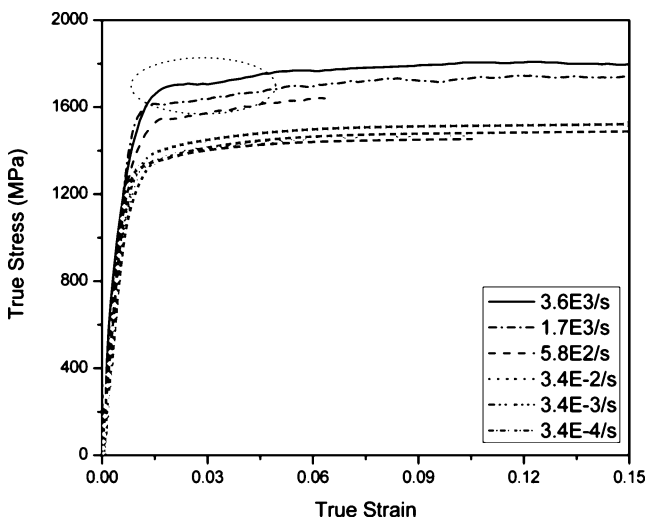


Fig. 6 True stress–strain curves of the 4340 steel at various dynamic and quasi-static strain rates

and quasi-static experiments. In Fig. 6, the stress at a certain strain increases with the strain rate increases from 3.4×10^{-4} to $3.6 \times 10^3 \text{ s}^{-1}$, indicating significant strain-rate effects. It is noted that only the portions beyond 0.015 strain in the stress–strain curve of $5.8 \times 10^2 \text{ s}^{-1}$, beyond 0.026 strain in the stress–strain curve of $1.7 \times 10^3 \text{ s}^{-1}$, and beyond 0.035 strain in the curve of $3.6 \times 10^3 \text{ s}^{-1}$ were obtained at constant strain rates. The strain of 0.015 is close to the yield strain for the material so that the plastic yield strength at the strain rate of $5.8 \times 10^2 \text{ s}^{-1}$ is considered reliable. However, the strains of 0.026 and 0.035 far exceed the strain of plastic yielding for the material. In the experiment of $3.6 \times 10^3 \text{ s}^{-1}$, the actual strain rate was only $2.5 \times 10^3 \text{ s}^{-1}$ rather than $3.6 \times 10^3 \text{ s}^{-1}$ when the specimen reaches the strain of 0.015 (Fig. 5). The strain rate in the strain range from 0.015 to 0.035 varied from $2.5 \times 10^3 \text{ s}^{-1}$ to $3.6 \times 10^3 \text{ s}^{-1}$ (Fig. 5). As a result, a lower early flow stress, as circled in Fig. 6, was measured during the experiment due to the lower initial strain rates; whereas, no such low early flow stress was observed in the stress–strain curve obtained at the lower constant plastic strain-rate of $5.8 \times 10^2 \text{ s}^{-1}$. Therefore, one cannot claim the strain rate at yielding to be $3.6 \times 10^3 \text{ s}^{-1}$. The yielding behavior does not represent the actual response of the material at the strain rate of $3.6 \times 10^3 \text{ s}^{-1}$.

We also conducted dynamic compressive experiments on another high strength, high toughness steel alloy, HP9-4-20 (9Ni-4Co-0.20C), supplied by Sandia National Laboratories, Livermore, CA. The dynamic experiments were conducted at two eventual constant strain rates: 1.3×10^3 and $4.9 \times 10^3 \text{ s}^{-1}$. The resultant stress–strain curves of these dynamic experiments are shown in Fig. 7. Figure 7 also shows a lower flow stress in the small plastic strain range (<0.07) in the stress–strain curve at the strain rate of $4.9 \times 10^3 \text{ s}^{-1}$. An obvious transitional trend in the stress–strain curve at this

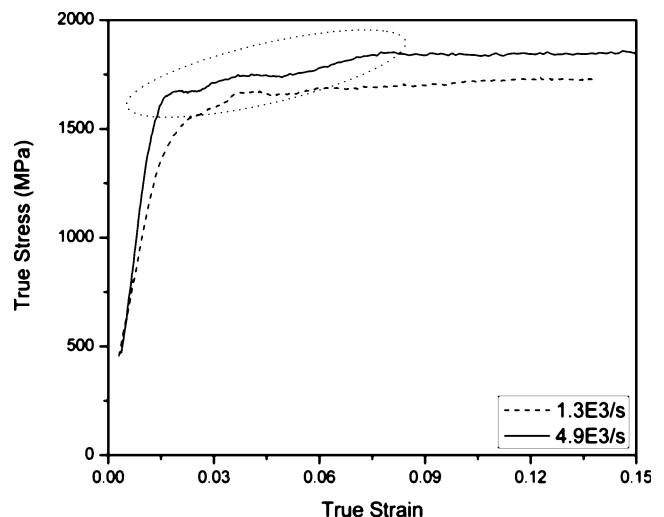


Fig. 7 True stress–strain curves of the HP9-4-20 steel alloy at two dynamic strain rates

Table 1 Material model constants

Constants	Values
Y	1,515 MPa
E	2×10^5 MPa
n	0.0328
α	195 MPa ($\dot{\varepsilon} \geq \dot{\varepsilon}_0$) 33 MPa ($\dot{\varepsilon} < \dot{\varepsilon}_0$)
$\dot{\varepsilon}_0$	$5.8 \times 10^2 \text{ s}^{-1}$

strain rate is observed, as indicated by the distinctive slope change pattern before and after the strain of 0.07. Therefore, an erroneous variation in dynamic yield strength with strain rates may be summarized when using such experimentally-measured data to determine the constants in the model.

It should be noted that, this phenomenon does not depend on the specimen length. Since the strain rate in the specimen is inversely proportional to the specimen length, it is possible to increase the strain rate in the specimen by using a smaller specimen and often a smaller bar [26]. The strain rate can be even as high as 10^4 s^{-1} in a torsion bar experiment [27]. However, as the strain rate in the smaller specimen increases from zero to a desired level, the strain accumulation in the specimen can easily exceed the yield strain of the specimen material, especially when the desired strain rate is very high (say, above 10^3 s^{-1}). It is therefore necessary to explore other approaches to obtain dynamic yield strength at high strain rates. In the next section, we attempt to employ an analytical model to indirectly approach the yield stress. The model's constants were determined using the experimental results during elastic and larger plastic deformation (beyond a few percent) of the material. An extrapolation is then created to cover the early plastic deformation range where the strain rate in the experiment cannot be maintained at a constant.

High-rate Compressive Stress–strain Relation of the 4340 Steel

In this section, we slightly modify an existing stress–strain relation developed by Warren and Forrestal [7] to describe the high-rate compressive response of the 4340 steel. This relation has been used and claimed efficient in numerical simulations for penetration phenomena [7]. The modified stress–strain relation in this research takes the form

$$\sigma = \begin{cases} E\varepsilon & \sigma \leq Y_d \\ Y \left(\frac{E\varepsilon}{Y_d} \right)^n + \alpha \log \left(\frac{\dot{\varepsilon}}{\dot{\varepsilon}_0} \right) & \sigma > Y_d \end{cases} \quad (4)$$

where σ is the Cauchy stress (true stress), ε is the logarithmic strain (true strain), n is the strain hardening

exponent, $\dot{\varepsilon}$ is the strain rate, E is Young's modulus, Y is the yield strength at the reference strain rate $\dot{\varepsilon}_0$, α is a curve fitting parameter with units of stress, and Y_d is the dynamic yield stress given by

$$Y_d = Y + \alpha \log \left(\frac{\dot{\varepsilon}}{\dot{\varepsilon}_0} \right) \quad (5)$$

This stress–strain relationship without many material constants is capable of serving the purpose of illustration in this study, even though a material model with more constants is believed to describe the experimental curves better. Since the stress–strain data at small strains are inaccurate, we used only the accurate portion in the stress–strain curves at various strain rates to determine the constants in the model [equation (4)]. In detail, we used the stress–strain data at the strains larger than 0.035 at the strain rate of $3.6 \times 10^3 \text{ s}^{-1}$, 0.026 at the strain rate of $1.7 \times 10^3 \text{ s}^{-1}$, and 0.015 at the strain rate of $5.8 \times 10^2 \text{ s}^{-1}$ as well as the entire quasi-static data to determine the constants. After curve-fitting, the values of the constants are listed in Table 1. Figure 8 presents the comparison of stress–strain curves determined from experiments and the model for the 4340 HRC45 steel. It is observed that the stress–strain relationship agrees well with the experimental data except for the data at small strains at the strain rates of 1.7×10^3 and $3.6 \times 10^3 \text{ s}^{-1}$ where the data were experimentally obtained at the lower strain rates than the claimed constants.

To verify the accuracy of the model, we also substituted the actual strain-rate history at the eventual strain rate of $3.6 \times 10^3 \text{ s}^{-1}$ (Fig. 5) into the stress–strain relation with the constants listed in Table 1 to predict what the stress–strain curve at this strain rate ($3.6 \times 10^3 \text{ s}^{-1}$) should be. The stress–strain curves as predicted by the model and as actually obtained from experiments are shown in Fig. 9. The close

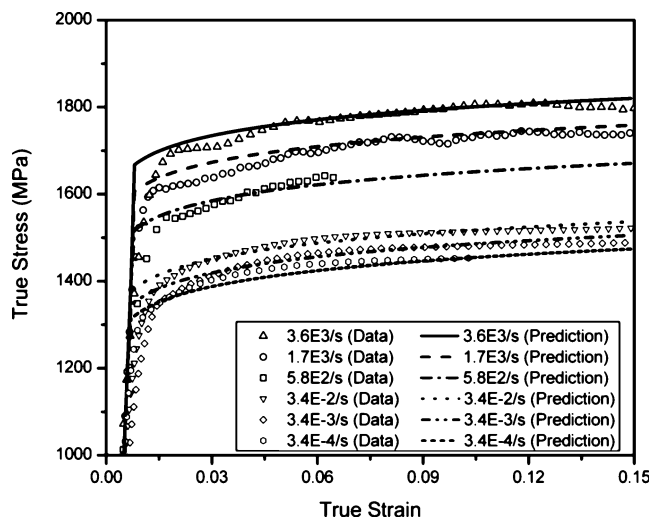


Fig. 8 Comparison of true stress–strain curves determined by experiments and constitutive relation

agreement between the prediction and the actual data in the early plastic deformation range indicates that the model describes the behavior of this material well. Furthermore, the stress–strain curve predicted by the stress–strain relation based on the assumed constant strain-rate history is also shown in Fig. 9. The curves based on these two different strain rate histories indicate that both stress–strain curves agree well when the strain is larger than 0.03, however, they are deviated from each other at small strains (<0.03) corresponding to the lower strain rate than claimed in this range. The yield stress provided by the stress–strain relationship assuming a constant (3600 s⁻¹) thus may be more accurate than the experimental value obtained at this “strain rate.” By way of details, the stresses at the strain of 0.01 are 1679 MPa predicted by the model and 1,493 MPa experimentally obtained by the experiment, respectively, the error of which is 12.5%. At the strain of 0.015, this error decreases to 2.5%, as shown in Fig. 9. The error of 12.5% for the very early flow stress at 0.01 strain is not acceptable when the strain rate effects of the material are desired to be accurately examined.

The experimental results and the analysis all indicate that, at relatively high strain rates, the measured yield strength and early flow stress for the ductile metal cannot be accurate. It is thus necessary to determine the upper strain-rate limit for obtaining reliable yield strength and early plastic flow stress. In the following section, we provide such an upper strain-rate limit through analysis.

Analysis of Upper Strain-rate Limit for Determining Yield Strength

We use the illustration in Fig. 10 to analyze the upper limit of the achievable constant strain rates at which the dynamic

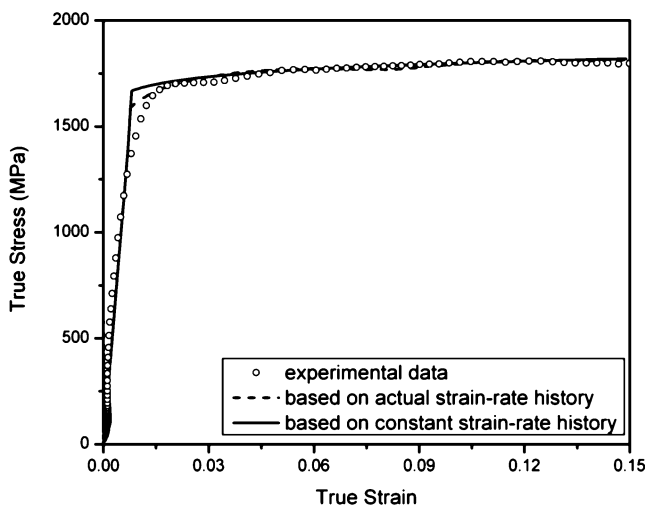


Fig. 9 Comparison of true stress–strain curves determined by experiment and the model on basis of actual strain-rate history and assumed constant strain rate, respectively

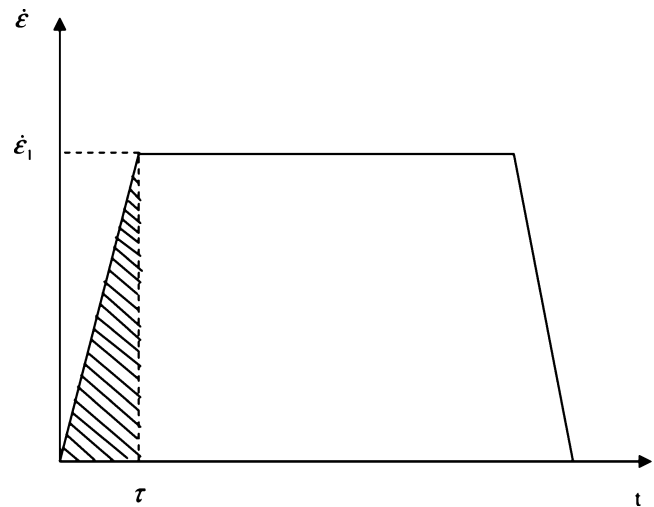


Fig. 10 Illustration of constant strain rate in specimen

yield strength for ductile materials can be unambiguously determined. Figure 10 displays a typical strain rate history experienced by a ductile specimen during the dynamic loading in a SHPB experiment. As illustrated in Fig. 10, the strain rate initially increases from zero until the time reaches τ when the strain rate starts to approach a constant value ($\dot{\epsilon}_0$). During this time τ , the strain in the specimen is accumulated to

$$\epsilon = \int_0^\tau \dot{\epsilon}(t) dt. \tag{6}$$

The history of the initial strain rate increase can be controlled by pulse shaping. For a metal in its elastic deformation, we can take a linear path for this history, i.e.,

$$\dot{\epsilon}(t) = a \cdot t \tag{7}$$

where a is a constant, $a = \dot{\epsilon}_1/\tau$. Substituting equation (7) into equation (6) yields

$$\epsilon = \frac{1}{2} a \cdot \tau^2 = \frac{1}{2} \dot{\epsilon}_1 \tau \tag{8}$$

The criterion for obtaining dynamic yield strength at the proposed strain rate, $\dot{\epsilon}_1$, is

$$\epsilon \leq \epsilon_Y \tag{9}$$

or

$$\dot{\epsilon}_1 \leq 2 \frac{\epsilon_Y}{\tau} \tag{10}$$

where ϵ_Y is the strain at the material’s dynamic yield strength. Therefore, the critical strain rate (upper strain-rate limit), $\dot{\epsilon}_{1c} = 2\epsilon_Y/\tau$, is determined by the yield strain of the material and the rise time (τ) in strain-rate history. Note that, for the purpose of producing an estimation, the strain rate effects on yield strains are not considered here, i.e., for a specific metal, the yield strain is taken as a constant. Since

the strain-rate history is represented by the reflected pulse when the specimen is at dynamic equilibrium, the rise time in the reflected pulse thus determines the upper strain-rate limit.

In a typical conventional SHPB experiment, the rise time in the incident pulse is approximately 10 μs ($\tau=10 \mu\text{s}$), which produces a reflected signal (or strain-rate history) with a rise time longer than 10 μs . It is noted that, during the initial few microseconds within the $\sim 10\text{-}\mu\text{s}$ rise time, the specimen is not in dynamic equilibrium. It takes several microseconds for the stress waves inside the specimen to “ring-up” to a state of nearly uniform stress. In this research, we use $\sigma_{0.2}=1,600 \text{ MPa}$ as the average yield strength. The yield strain (ε_y) for the materials is, $\varepsilon_y = 0.002 + \sigma_{0.2}/E = 0.01$, on basis of elastic modulus of 200 GPa. According to equation (10), the upper strain-rate limit is estimated to be $\dot{\varepsilon}_{0c} = 2\varepsilon_y/\tau = 2000 \text{ s}^{-1}$. This means that it is not feasible to obtain yield strength at the strain rates above $2,000 \text{ s}^{-1}$ for this material. It is noted that the yield strain in equation (10) may be strain rate dependent or independent. Here we estimated the limit on basis of no rate dependence, which provides an estimation of the strain rate limit. Using a strain-rate-dependent model certainly provides a more accurate estimation of the strain rate limit.

A smaller-diameter SHPB can produce incident pulses with shorter rise times, i.e., 5 μs , (but not at a difference of an order of magnitude) [26], which in turn can facilitate high upper limit of strain rate for obtaining dynamic yield strength. However, as the bar diameter decreases, so does the specimen size, which has a lower limit for representing bulk material behavior. When pulse shapers are used in the SHPB experiments for the purpose of achievement of constant strain rate in specimen, the initial loading rate of the incident pulse is typically lowered such that the rise time increases, resulting in longer rise time in strain-rate history. The rise time in the reflected pulses obtained from such a pulse-shaped SHPB experiment could be at least twice (20 μs) as that obtained from a conventional SHPB experiment. The upper strain-rate limit thus becomes only half ($1,000 \text{ s}^{-1}$) of that in a conventional SHPB. Therefore, the pulse shaping techniques, which are very effective in producing constant-strain-rate deformation in the specimen under dynamic equilibrium, limits the upper end of the strain-rate range in which yield strength can be accurately determined. Thus, when the SHPB (with or without pulse shaping) is used for characterizing ductile materials at very high strain rates, the validity of yield strength and early flow stress should be carefully examined.

Conclusions

To accurately determine the yield strength and flow stress of a specimen material as a function of strain rates, the strain

rate in each experiment needs to be maintained constant over the loading duration. However, the strain rate in the specimen has to increase from zero to this constant in a dynamic experiment. The strain accumulated over this initial period of the experiment may exceed the yield strain of the material. In this study, we conducted dynamic experiments on high-strength steel alloys at high strain rates with a pulse-shaping SHPB and examined the validity of dynamic yield strength and early plastic flow stress results at various high strain rates. It is experimentally shown that the specimen yields before the strain rate reaches the desired constant value during high-rate experiments. In such experiments, the strain rates corresponding to plastic yielding and early plastic flow are lower than the desired constant value, leading to significant errors in the results for strain-rate sensitive materials. This affects the modeling of the dynamic experimental results. As an example, an existing rate-dependent stress–strain relationship was used to estimate the true yield strength at high strain rates. The upper strain-rate limit for obtaining reliable yield strength at high strain rates was also estimated.

Acknowledgments This work was supported by Sandia National Laboratories, Albuquerque, NM and Livermore, CA. Sandia is a multiprogram laboratory operated by Sandia Corporation, a Lockheed Martin Company, for the United States Department of Energy under Contract DE-AC04-94AL8500.

References

- Zukas JA, Nicholas T, Swift HF, Greszczuk LB, Curran DR (1992) Impact dynamics. Krieger, Malabar, FL.
- Rajendran AM, Bless SJ, Dawicke DS (1986) Evaluation of Bodner-Partom model parameters at high-strain rate. *Exp Mech* 26:319–323.
- Liang R, Khan AS (1999) A critical review of experimental results and constitutive models for BCC and FCC metals over a wide range of strain rates and temperatures. *Int J Plast* 15:963–980.
- Khan AS, Zhang H (2000) Mechanically alloyed nanocrystalline iron and copper mixture: behavior and constitutive modeling over a wide range of strain rates. *Int J Plast* 16:1477–1492.
- Lindholm US (1964) Some experiments with the split Hopkinson pressure bar. *J Mech Phys Solids* 12:317–335.
- Rajendran AM, Garrett RK, Clark JB Jr, Jungling TL (1991) Effects of strain rate on plastic flow and fracture in pure tantalum. *J Mater Shap Technol* 9:7–20.
- Warren TL, Forrestal MJ (1998) Effects of strain hardening and strain-rate sensitivity on the penetration of aluminum targets with spherical-nosed rods. *Int J Impact Eng* 35:3737–3753.
- Rittel D, Ravichandran G, Lee S (2002) Large strain constitutive behavior of OFHC copper over a wide range of strain rates using the shear compression specimen. *Mech Mater* 34:627–642.
- Krempf E, Khan F (2003) Rate (time)-dependent deformation behavior: an overview of some properties of metals and solid polymers. *Int J Plast* 19:1069–1095.
- Khan AS, Suh YS, Kazmi R (2004) Quasi-static and dynamic loading responses and constitutive modeling of titanium alloys. *Int J Plast* 20:2233–2248.

11. Frew DJ, Forrestal MJ, Chen W (2002) Pulse shaping techniques for testing brittle materials with a split Hopkinson pressure bar. *Exp Mech* 42:93–106.
12. Frew DJ, Forrestal MJ, Chen W (2005) Pulse shaping techniques for testing elastic-plastic materials with a split Hopkinson pressure bar. *Exp Mech* 45:186–195.
13. Duffy J, Campbell JD, Hawley RH (1971) On the use of a torsional split Hopkinson bar to study rate effects in 1100-0 aluminum (ASME Transactions). *J Appl Mech* 37:83–91.
14. Chen W, Song B, Frew DJ, Forrestal MJ (2003) Dynamic small strain measurements of a metal specimen with a split Hopkinson pressure bar. *Exp Mech* 43:20–23.
15. Meyers MA (1994) *Dynamic behavior of materials*. Wiley, New York.
16. Gray G (2000) Classic split-Hopkinson pressure bar testing. In: *Mechanical testing and evaluation, ASM handbook*. ASM, Materials Park, OH, pp 462–476.
17. Ellwood S, Griffiths LJ, Parry DJ (1982) Materials testing at high constant strain rates. *J Phys E Sci Instrum* 15:280–282.
18. Leroy M, Raad MK, Nkule L, Cheron R (1984) Influence of instantaneous dynamic decremental/incremental strain rate tests on the mechanical behavior of metals—application to high-purity polycrystalline aluminum. In: *3rd conference of mechanical properties at high rates of strain 70*, pp 31–38.
19. Kobayashi H, Daimaruya M, Nojima T, Kajino T (2000) Effect of strain rate change during uniaxial dynamic tensile tests on instability strain. *J Phys IV (France)* 10:Pr9-433–438.
20. Nojima T, Ogawa K (1985) New applications of split Hopkinson bar to materials testing. *J Phys Colloq C5*:623–631.
21. Song B, Chen W, Weerasooriya T (2003) Quasi-static and dynamic compressive behaviors of a S-2 glass/SC15 composite. *J Compos Mater* 37:1723–1743.
22. Song B, Chen W (2004) Loading and unloading SHPB pulse shaping techniques for dynamic hysteretic loops. *Exp Mech* 44:622–627.
23. Pan Y, Chen W, Song B (2005) The upper limit of constant strain rate in a split Hopkinson pressure bar experiment. *Exp Mech* 45:440–446.
24. Song B, Chen WW, Dou S, Winfree NA, Kang JH (2005) Strain-rate effects on elastic and early cell-collapse responses of a polystyrene foam. *Int J Impact Eng* 31:509–521.
25. Ramesh KT, Narasimhan S (1996) Finite deformations and the dynamic measurement of radial strains in compression Kolsky bar experiments. *Int J Solids Struct* 33:3723–3738.
26. Jia D, Ramesh KT (2004) A rigorous assessment of the benefits of miniaturization in the Kolsky bar system. *Exp Mech* 44:445–454.
27. Gilat A, Cheng CS (2002) Modeling torsional split Hopkinson bar tests at strain rates above $10,000 \text{ s}^{-1}$. *Int J Plast* 18:787–799.